The value of T for Alouette I, which employs 1-in.-diam steel STEMs with properties listed in Table 1, is 11.5 sec. For Alouette II and ISIS-I, employing beryllium copper 0.5-in.-diam STEMs, T of Eq. (20) is 1.3 sec.

Concluding Remarks

The experimental and analytical evidence strongly indicate that the appropriate time constant for despin theories is as given by Eq. (20). Allowing for variation in radius (it appears that the radius of STEMs slightly increases over a period of years) and other parameters, it appears that the upper bound values of T for satellite applications are about 1.6 and 14 sec for beryllium copper and steel STEMs, respectively.

References

[1] Etkin, B. and Hughes, P. C., "Spin Decay of a Class of Satellites Caused by Solar Radiation," Rept. 107, July 1965, Univ. of Toronto, Institute for Aerospace Studies (UTIAS).

[2] Etkin, B. and Hughes, P. C., "Explanation of the Anomalous Spin Behaviour of Satellites with Long Flexible Antennas," *Journal of Spacecraft*, Vol. 4, No. 9, Sept. 1967, pp. 1139–1145.

[3] Gerrish, R. J., "Thermal Bending Response Times for Alouette I and Alouette B Sounder Antennae," private communication, 1965, Ottawa, Canada.

[4] Vigneron, F. R., "Experiments on Lateral Vibrations of Alouette Sounder Antennas," DRTE Rept. 1170, Nov. 1966, Dept. of National Defence, Ottawa, Canada.

[5] Mar, J. and Garrett, T., "Mechanical Design and Dynamics of the Alouette Spacecraft," *Proceedings of IEEE*, Vol. 57, No. 6, June 1969, pp. 882–896.

[6] Paghis, I., Franklin, C. A., and Mar, J., "Alouette I, The First Three Years in Orbit," DRTE Rept. 1159, March 1967, Dept. of National Defence, Ottawa, Canada.

[7] Boley, B. A. and Weiner, J. H., *Theory of Thermal Stresses*, Wiley, New York, 1960, pp. 307–314.

[8] Vigneron, F. R., "Transient Temperature and Thermal Curvature Behavior of Sounder Antennas on Alouette Satellites," DRTE Rept. 1167, Nov. 1966, Dept. of National Defence, Ottawa, Canada.

Prediction of Interstitial Gas Pressure in Multilayer Insulation during Rapid Evacuation

K. M. Kneisel* and F. O. Bennett†
Convair Division of General Dynamics, San Diego, Calif.

THE use of multiple-layer radiation shields for insulating cryogenic propellant tanks on long-term missions has long been considered. However, the fragile nature of the shields ($\frac{1}{4}$-mil aluminized Mylar) has necessitated a considerable development program for designing a light weight, structurally sound insulation system. One problem has been the prediction of the insulation stresses caused by the evacuation of the helium purge gas during ascent. These stresses can be estimated for a particular shape blanket using membrane theory if the pressure differential across the blanket can be determined.

The gas flow in most multilayer blankets is two-dimensional; however, a conservative estimate of the pressure differential can be made using the results of one-dimensional theory wherein the minimum linear flow path (distance from center of blanket to the nearest open edge) is used as the length dimension.

Presented as Paper 69-608 at the AIAA 4th Thermophysics Conference, San Francisco, Calif., June 16–18, 1969; submitted May 13, 1970; revision received July 1, 1970. This work was sponsored by NASA/MSFC on Contract NAS 8-18021 under the direction of E. H. Hyde.

* Senior Thermodynamics Engineer, Thermodynamics Group.
† Thermodynamics Engineer, Thermodynamics Group.

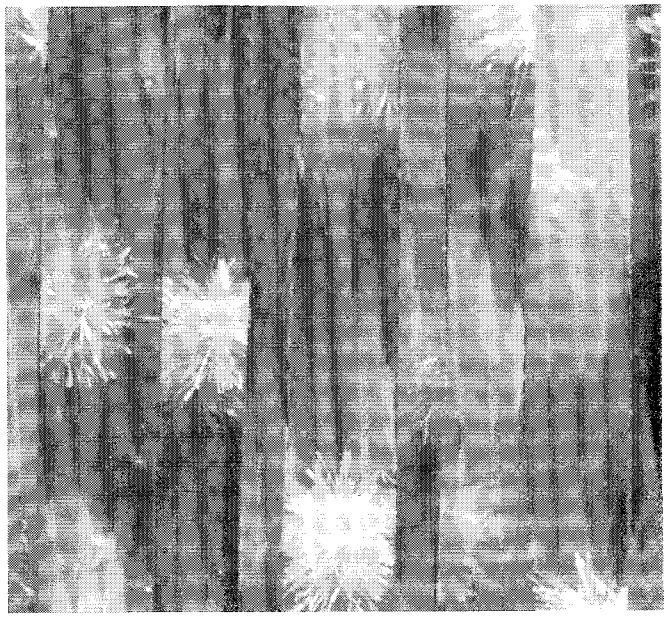

Fig. 1 Layers of Superfloc.

In multilayer insulation blankets, adjacent shields are spaced either by use of positive low-conductive spacers such as foam sheets, or by deforming each shield so that adjacent shields touch only over a minimal area. The effect of these spacers on the gas flow makes the flow problem too complex to solve analytically without empirical data. Therefore, we postulate a type of flow and force the solution of the analytical model to fit experimental data with the use of a correlation factor. This factor is a function o the layer density only for each particular type of insulation. The type of in ulation tested in this study was Superfloc (Fig. 1). In this insulation, the spacer consists of small tufts of Dacron needles.

Analytical Model

We assume that the gas flow is analogous to continuum flow in a porous medium with constant permeability; it is one dimensional and isothermal; and the gas is perfect with constant fluid properties.

The mass flow rate is given by the equation $\dot{m} = (K/\mu) \times \rho(\partial P/\partial x)$ where μ is the mean gas viscosity evaluated at the average blanket temperature. K is the insulation permeability and is a function of layer density only. It is to be determined experimentally for each type of insulation.

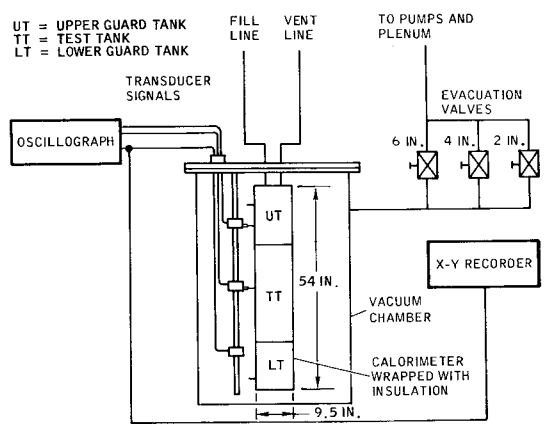

Fig. 2 Experimental apparatus schematic.

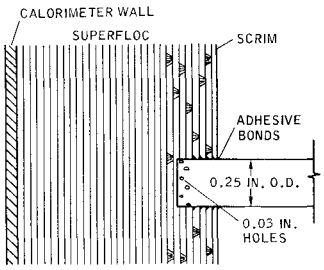

Fig. 3 Pressure probe mounting arrangement in Superfloc insulation.

If a mass balance is performed on a differential control element in the insulation, the following equations result.

$$(K/\mu)\ \partial/\partial x\ (\rho \partial P/\partial x) = \partial\rho/\partial t \tag{1}$$

Since the gas is assumed perfect, $\rho = (P/RT)$, and

$$(\mu/K)\ \partial P/\partial t = \partial/\partial x\ (P\ \partial P/\partial x) \tag{2}$$

We impose the following on Eq. (2):

Boundary conditions: $P(L,t) = P_a(t)$; $(\partial P/\partial x)\ (0, t) = 0$ — Initial condition: $P(x, 0) = P_0$ (3)

where $x = 0$ is the middle, no-flow location, of the blanket; $x = L$ is the open end of the blanket; $P_a(t)$ is the ambient pressure; and P_0 is the initial pressure.

The equation for the pressure differential may be derived with the substitution

$$\eta(x, t) = P(x, t) - P_a(t)$$

Then

$$(\mu/K)\ [(\partial\eta/\partial t) + P_a'(t)] = [\eta + P_a(t)]\ (\partial^2\eta/\partial x^2) + (\partial\eta/\partial x)^2 \tag{4}$$

Boundary conditions: $\eta(L, t) = 0$; $(\partial\eta/\partial x)\ (0, t) = 0$ — Initial condition: $\eta(x, 0) = 0$ (5)

Equation (4), with boundary and initial conditions given by Eq. (5), completed the statement of the mathematical model. This model was solved numerically using an implicit difference method and the CDC 6400 digital computer.

Experimental Program

The apparatus consisted of a 9.5-in.-diam, 54-in.-long copper cryogen tank and a 36-in.-diam vacuum chamber (Fig. 2).

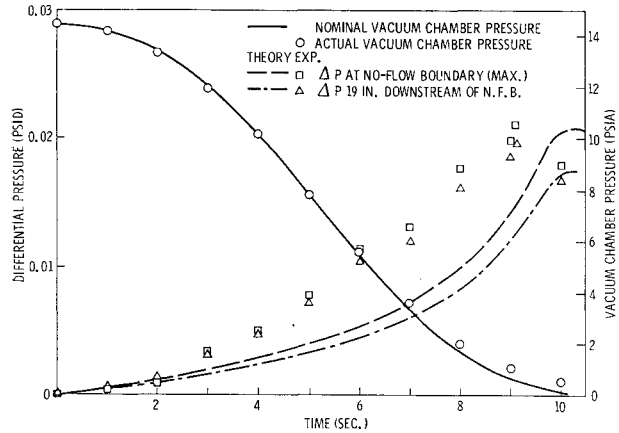

Fig. 4 Pressure transducer output from a typical run—also shown are the corresponding solutions to Eqs. (4) and (5): 30 layers/in.; 46-in. evacuation length; 535°R sink temperature; 10X nominal Saturn pressure profile.

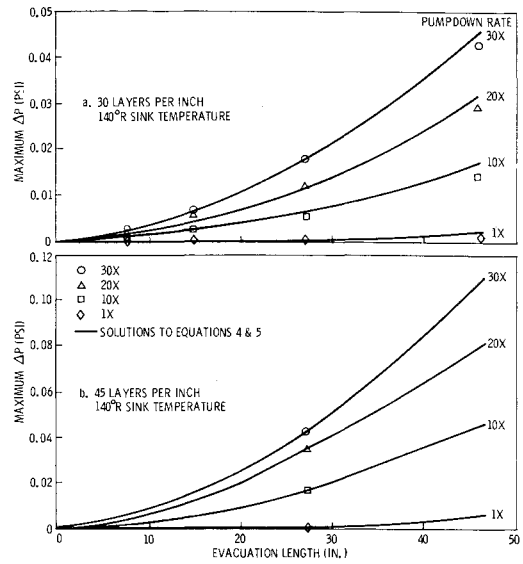

Fig. 5 Variation of maximum pressure differential with evacuation length and pumpdown rate—Superfloc 30 and 45 layers/in.

The tank was wrapped with 1 in. of insulation at densities of 30 and 45 layers/in. One layer of Schjeldahl X-850 scrim reinforced Mylar was wrapped around the outside to prevent deformation and bulging of the insulation. Pressure probes were embedded (Fig. 3) at four locations along the length. Two variable reluctance pressure transducers (0–0.5 psid) were used to measure the differential pressure across the outer layers of the insulation. These transducers were calibrated statically for the range 0.009–0.15 psid and had a maximum of 5% of reading error. A third variable reluctance transducer measured the vacuum chamber pressure.

One transducer was positioned at the "no flow" or maximum-pressure differential location which is located at the center of the blanket when both ends of the blanket are open. The other was located at a position corresponding to approximately one-half of the total evacuation length. By cutting and banding the insulation, evacuation lengths of 46, 27, 14, and 8 in. were obtained.

The evacuation pressure profiles were scaled to a nominal Saturn launch profile. Pumpdown rates of 1, 10, 20, and 30 times that of the nominal profile were performed. Three insulation sink temperatures of 535° R, 140°R, and 37°R and a single-source temperature of 535°R were used to investigate the effect of the helium purge gas viscosity on insulation evacuation rate.

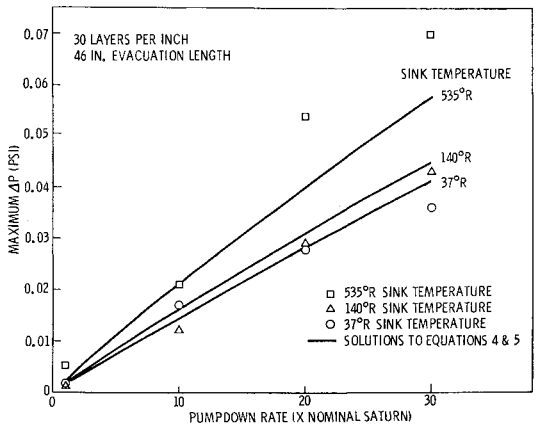

Fig. 6 Variation of maximum pressure differential with temperature—Superfloc 30 layers/in.

To obtain the desired vacuum chamber pressure history, predetermined pressure profiles were used on a Moseley X-Y recorder. Three evacuation valves were manually operated so that the recorder pen followed the plotted curve during pumpdown (Fig. 2). At the higher pumpdown rates, it usually took several tries before an acceptable chamber pressure history was obtained. Times to evacuate the vacuum chamber from ambient pressure to 0.25 psia ranged from 105 to 3.5 sec, and the transducer output signals were recorded on a high-frequency Honeywell oscillograph.

Test Results and Correlation with Theory

The data from a typical run are shown in Fig. 4. This graph shows the actual and nominal vacuum chamber pressure histories together with the output of the two differential pressure transducers. Also shown are the theoretical predictions from the solution to Eqs. (4) and (5). A value of the permeability K was chosen so that the solution would match the value of the maximum measured pressure differential at the no-flow boundary. In Fig. 4, the theoretical pressure differential curve for the location 19 in. downstream of the no-flow boundary was generated by using the same value of K chosen for the NFB case. The viscosity was always evaluated at the average of the chamber and tank temperatures. The value of K for a specific layer density was then obtained by averaging the values for each run. This was done extensively for the 30 layers/in. density where four different evacuation lengths, four pumpdown rates, and three mean temperatures were used. The following values were derived for the two-layer densities: $K = 1.47 \times 10^{-6}\text{ft}^2$, for Superfloc at 30 layers/in. and $K = 5.01 \times 10^{-7}\text{ft}^2$, for Superfloc at 45 layers/in.

For design purposes, the maximum pressure differential is usually the parameter of interest. Figure 5 presents these data as a function of evacuation length and ambient pressure history. Figure 6 shows the effect of viscosity (temperature). It can be observed that the model does not correlate well over a wide temperature range (280°–535°R). It should be noted that all test points were used in the calculation of the permeability K. If the points at the higher mean temperature (535°R) were deleted, the correlations of $\Delta P_{\max}$ vs L presented in Fig. 5 would be closer.

Derivation of the Quaternion Scheme via the Euler Axis and Angle

CARL GRUBIN*
Hughes Aircraft Company, Culver City, Calif.

A QUATERNION is a four-parameter system for uniquely specifying the attitude of a rigid body with respect to some reference frame. The four parameters themselves are determined by solving the quaternion-rate equations, which are linear differential equations whose coefficients are the body angular rates. Once the parameters are determined, the elements of the direction-cosine matrix that determine the body attitude can be formulated. In this Note the direction cosine matrix in terms of the quaternion parameters and the quaternion-rate equations are both derived in a simple physical way using the concept of the Euler axis and angle. A supplementary result of these derivations is an explicit solution for the initial quaternion in terms of the initial direction cosines.

Received June 3, 1970.

* Senior Staff Engineer, Aeronautical Systems Division. Associate Fellow, AIAA.

Analysis

A theorem due to Euler states (in effect) that any sequence of rotations of a rigid body which has one point fixed can be arrived at by a single rotation—the Euler angle (Author's nomenclature)—about some axis—the Euler axis (Author's nomenclature)—which passes through the fixed point.[1] Let the fixed point in the body be located at the origin of a set of fixed Cartesian axes X, Y, Z, with unit vectors $\mathbf{I}$, $\mathbf{J}$, $\mathbf{K}$. Introduce a second set of Cartesian axes x, y, z, with unit vectors $\mathbf{i}$, $\mathbf{j}$, $\mathbf{k}$, which are fixed in the body. Let the angular velocity of the body at any time, $\boldsymbol{\omega}$, be described by components p, q, r measured along x, y, z. Then

$$\boldsymbol{\omega} = \mathbf{i}p + \mathbf{j}q + \mathbf{k}r \tag{1}$$

where p, q, r are assumed to be known time functions.

Now the time history of p, q, r integrated from $t = 0$ to the present time $t = t$ has brought the rigid body from the reference attitude—x, y, z coincident with X, Y, Z—to its present attitude. By Euler's theorem this sequence of motions is equivalent to a single rotation θ about some well-defined axis which passes through the origin. Let this axis be defined by a unit vector $\mathbf{e}_\theta$, with the rotation θ around $\mathbf{e}_\theta$ taken positive in the sense of the right hand convention. Initially, the viewpoint is that $\mathbf{e}_\theta$ and θ are known and the first problem is to calculate the transformation matrix between X, Y, Z and x, y, z. Later, equations are developed for determining $\mathbf{e}_\theta$ and θ given the time history of p, q, r.

The transformation matrix can be obtained by applying a general formula for rigid-body rotation derived earlier.[2] Using this formula one can determine the final orientation of any line in a rigid body, which intersects a fixed axis, when the rigid body undergoes a finite rotation about this axis (Fig. 1). The result is

$$\mathbf{r}_f = \mathbf{r}_0(\cos\theta) + \mathbf{e}_\theta(\mathbf{e}_\theta \cdot \mathbf{r}_0)(1 - \cos\theta) + (\mathbf{e}_\theta \times \mathbf{r}_0)\sin\theta \tag{2}$$

where $\mathbf{e}_\theta$ = unit vector along the axis of rotation, θ = rotation angle, and $\mathbf{r}_0$, $\mathbf{r}_f$ = initial and final orientations of the line.

In the present paper the axis-angle combination is again designated by $\mathbf{e}_\theta$ and θ, so Eq. (2) can be applied directly by substituting the appropriate axes for $\mathbf{r}_0$ and $\mathbf{r}_f$. Thus, to find the direction cosines for unit vector $\mathbf{i}$, take

$$\mathbf{r}_f = \mathbf{i} \text{ and } \mathbf{r}_0 = \mathbf{i}_0 = \mathbf{I} \tag{3}$$

since at the start of every rotation x is coincident with X.

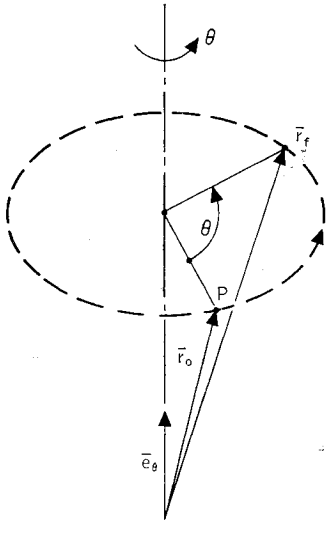

Fig. 1 Finite rotation.